Direct monitoring of minority carrier density during light induced degradation in Czochralski silicon by photoluminescence imaging

Tine Uberg Naerland, Hallvard Angelskår, and Erik Stensrud Marstein

Citation: Journal of Applied Physics **113**, 193707 (2013);
View online: https://doi.org/10.1063/1.4806999
View Table of Contents: http://aip.scitation.org/toc/jap/113/19
Published by the American Institute of Physics

Direct monitoring of minority carrier density during light induced degradation in Czochralski silicon by photoluminescence imaging

Tine Uberg Naerland,[1,2,a)] Hallvard Angelskår,[1] and Erik Stensrud Marstein[1]
[1]*Institute for Energy Technology, Instituttveien 18, 2007 Kjeller, Norway*
[2]*Department of Material Science and Engineering, NTNU, 7491 Trondheim, Norway*

(Received 12 February 2013; accepted 2 May 2013; published online 20 May 2013)

In this paper, we present a new method for studying the light induced degradation process, in which the minority carrier density is monitored directly during light soaking by photoluminescence imaging. We show experimentally that above a certain minority carrier concentration limit, Δn_{lim}, the boron oxygen (B-O) defect generation rate is fully independent of the injected carrier concentration. By simulation, we determine Δn_{lim} for a range of p-type Czochralski silicon samples with different boron concentrations. The normalized defect concentrations, N_t^*, are determined for the same samples by time-resolved Quasi Steady State Photoconductance measurements. After 10 min of light degradation, no correlation between Δn_{lim}, and N_t^* is observed. These results indicate that the role of the excess carriers during the rapid decay is to first change the charge state of the defects by shifting the electron quasi-Fermi level across the energy level of the defect centre in its passive state ($E_{lat} = E_V + (635 \pm 18)$ meV) and that, subsequently, another rate-determining step proceeds before the defect centre becomes recombination active. © *2013 AIP Publishing LLC*. [http://dx.doi.org/10.1063/1.4806999]

I. INTRODUCTION

Severe lifetime reduction with carrier injection is an unfortunate characteristic of p-type Czochralski silicon materials. During a time period of a day or less, the electron lifetime is typically reduced to about 10% of the initial lifetime. The lifetime reduction is attributed to a recombination centre that becomes activated by charge carriers.[1] Two exponential decay processes, one rapid and one slow, describe the degradation kinetics. Both decays are found to be related to the simultaneous presence of oxygen and boron in the Si material, through a possible boron-oxygen defect (B-O defect),[2] but neither the chemical composition nor the energy level of the defect has so far been determined experimentally. It has been shown that the rates of the rapid and slow degradation are proportional to the square of the boron concentration [B],[2] while they are independent of the oxygen concentration.[2] The role of the excess carriers has, however, not been studied in detail.

In the model of Schmidt *et al.*, the role of the excess minority carriers in the defect generation were believed not to be directly involved in the defect reaction, but their presence was thought to trigger the reaction by (i) charging the state of the O_{2i}, which might lead to an increase in the O_{2i} diffusivity; or (ii) enhancing the O_{2i} diffusivity via a recombination-enhanced diffusion process.[3] Recent work published in 2011[4] stated, however, that this type of motion of an oxygen dimer is a highly unlikely mechanism in solar grade silicon. Accordingly, this hypothesis disputed the role of the excess carriers in the model.

In 2010/2011, Voronkov and Falster[5,6] proposed a new degradation model wherein a latent recombination centre is already incorporated in the crystal before carrier injection. According to this model, the centres responsible for the slow and rapid lifetime decays are B_iO_{2i} and B_sO_{2i}, respectively. In p-type silicon, the activation of B_sO_{2i} (defect centre responsible for the rapid lifetime decay) is explained through a series of steps where the quadratic proportionality between hole concentration and lifetime is accounted for by the capture of holes by a negative latent centre. The positive latent centre is then reconstructed into a transient centre. One of the final transitions leading to the formation of a recombination-active centre is a de-charging of the transient centre from positive to neutral by electron injection.

Commonly, the light induced degradation (LID) is monitored either by Microwave Photo Conductance Decay (μw-PCD) or Quasi Steady State Photo Conductance (QSSPC) lifetime measurements of a sample during light exposure or by measuring the change in open circuit voltage (V_{OC}) of a solar cell being subjected to an applied forward bias. However, none of these methods retain the information of the minority carrier density in the sample during the extended light exposure or applied forward bias treatments. It has been shown that very low carrier density levels are sufficient to activate the recombination centres,[7,8] but the degradation process is, nevertheless, completely reliant on increased carrier densities.[8] If the injection or heat source is removed, the degradation will cease immediately. Several groups have studied the influence of varying illumination intensity on the B-O defect generation rate. These studies[9,10] have shown that the generation rate of the defect saturates at a certain illumination intensity. For highly degradable material, i.e., material with high concentrations of boron and oxygen, the defect generation rate saturates at about 1 mW/cm^2. The intensity of the illumination source and the excess

a)Author to whom correspondence should be addressed. Electronic mail: tine.narland@material.ntnu.no. Tel.: +47 99 04 05 08. Fax: +47 63 89 99 64.

carrier density is linked through the optical properties of the sample and the carrier lifetime. A certain illumination intensity threshold value therefore corresponds to a certain excess carrier threshold value, Δn_{lim}, but the same illumination intensity gives widely different excess carrier densities for different materials.

In this work, we experimentally demonstrate that such an excess carrier threshold value, Δn_{lim}, exists and that above Δn_{lim} the generation rate is fully independent of carrier concentration. These findings are uncovered by a new way of studying the LID process, in which the excess carrier density is monitored directly during the light soaking. Local light induced defect generation, wherein the wafer is exposed to light in a confined area, causes the excess electrons to diffuse out into the wafer, allowing us to study the degradation effect of a continuously varying electron concentration. This concentration can be monitored by means of photoluminescence (PL) imaging. By applying simulations for the very low carrier concentrations, we are able to quantify Δn_{lim}. The procedure is performed on a series of samples and the results are used to investigate whether there is a correlation between Δn_{lim} and the B-O defect density. Finally, we discuss whether the role of the excess carriers is to simply shift the quasi-Fermi energy causing a charge state change.

II. EXPERIMENTAL METHODS

The samples used in this study are boron doped Cz-Si wafers with a boron concentration ranging from 3.5×10^{15} to $8.5 \times 10^{15}\,\text{cm}^{-3}$. Prior to the measurements, the wafers were cleaned with RCA and thereafter received a double side passivation by plasma-enhanced chemical-vapor deposited (PECVD) hydrogenated amorphous silicon (a-Si:H). a-Si:H passivation has the advantage compared to silicon nitride (a-SiN$_x$:H) passivation that no inversion channel is formed on p-type material. An inversion channel could possibly introduce a smearing effect on the PL signal detected by the camera.[11] The a-Si:H.-passivation still provides an excellent and stable level of surface passivation with a surface recombination velocity below 40 cm/s. In order to ensure that no defect centres are generated before the start of the measurements, the samples were deactivated by an annealing at 210 °C for 15 min on a hotplate.[2]

The B-O defect densities are determined by time resolved lifetime measurements. The lifetime degradation was monitored by a custom built, automated QSSPC setup using an externally controlled bias lamp for in-situ illumination between measurements. The bias light source was a halogen lamp with an intensity of approximately 50 mW/cm. The temperature of the sample was monitored by a thermistor coupled to the sample stage, but the temperature change of the stage and sample due to illumination was not significant for the measured lifetime. According to Shockley Read Hall theory,[12] the defect concentration can be directly related to the lifetime, provided that the generated defects are the dominating recombination mechanism. The normalized defect concentration, N_t^*, is related to the measured lifetime by the following equation $N_t^*(t) = 1/\tau(t) - 1/\tau(0)$ where $\tau(0)$ is the initial carrier lifetime before LID and $\tau(t)$ is the carrier lifetime after a certain exposure time.[13] The lifetimes were measured at a fixed injection level corresponding to one tenth of the doping level for each sample, respectively.[2]

The PL measurements were performed with a LIS-R1 system from BTimaging. In the chamber, a 4.5 mW diode laser with a wavelength of 780 nm was installed in order to illuminate a specific area of the wafer. A principle sketch of the setup is given in Fig. 1. The laser beam was shaped and focused into a narrow line with a Gaussian half width of $50 \pm 5\,\mu$m. The incidence angle was set to 10° to avoid detection of the specular reflection from the laser beam by the charge-coupled device (CCD) camera. When the laser is turned on, the generated carriers will diffuse from the illuminated area into the adjacent area following the continuity equation. In silicon containing boron and oxygen, the diffusing carriers generate B-O defects that reduce the lifetime far beyond the borders of the illuminated area. As the concentration of B-O defects increases with time, the diffusion length of the carriers decreases. This can easily be observed by imaging the PL generated from a localized area in a p-type Cz-Si sample at $t = 0$ and $t \neq 0$, see Fig. 2.

The laser shown in Fig. 1 has two functions. One is to provide enough excess carriers over time to create an area of reduced lifetime, visible as a groove-shaped feature in the lifetime maps. The other is to act as an excitation source during the PL measurements of direct monitoring of minority carrier density with local excitation, which in principle can be performed on any type of silicon material. As discussed in the introduction, the B-O defect *generation rate* is independent of carrier concentration above a certain value, Δn_{lim}. Therefore, a lifetime plateau in the bottom of the generated lifetime groove-shaped profile is formed. In Fig. 3, a principle sketch of approximately one half of the lifetime profile is shown. The four regions correspond to the degraded region, the exposed region, the transition region, and the unaffected region. Looking at the charge carrier concentration profile for an arbitrary time ($t \neq 0$), the carriers that are generated in the exposed region will be subject to a uniform diffusion length in the already degraded region. However, upon reaching the transition region, the lifetime will rapidly change to the better. This will appear as a change in the slope of the

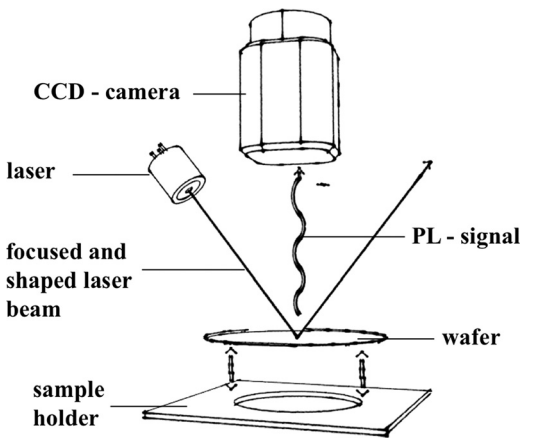

FIG. 1. Sketch showing the setup for direct monitoring of excess carrier density during light induced degradation. The wafer is exposed to a focused and shaped laser beam while the PL signal is collected by a CCD camera.

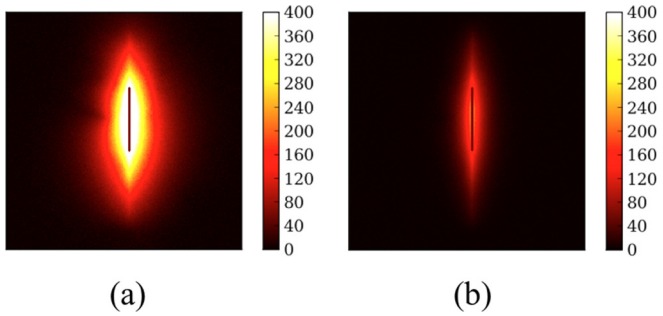

FIG. 2. PL intensity data (normalized to exposure time) taken (a) immediately when the light soaking is started, t = 0 and (b) after light soaking for t = 3 min. The position and width of the exposed area are superimposed on the image, as indicated by the vertical grey line. Data acquisition time is 0.5 s. By comparing the images, it is obvious that the carrier density decreases with increased time of light exposure. This is due to the shorter minority carrier lifetime caused by the generation of B-O defects.

spatial carrier concentration profile in the transition region. The carrier concentration that corresponds to this change in the slope is thus the carrier concentration limit value, Δn_{lim}, where the defect generation rate becomes saturated.

In the present work, we illuminated the material with a focused, low-flux laser for 10 min (peak photon flux, $\phi_{low} = 2.9 \times 10^{16}\,\mathrm{s}^{-1}\,\mathrm{cm}^{-2}$). After 10 min, a groove-shaped lifetime profile is formed and an image of the spatial carrier profile was taken. Unfortunately, the CCD camera cannot detect a PL signal low enough to directly observe the carrier concentrations in the transition region. With a larger carrier concentration (increased excitation), the effect can, however, be seen on the spatial carrier profile. A high photon flux will thus demonstrate the change in the slope on the carrier profile but will not represent the carrier concentration that was responsible for creating the defects. In order to determine the actual Δn_{lim} where the defect generation rate becomes saturated we have simulated the spatial carrier profile for these low carrier concentrations. The procedure will be described in Sec. III.

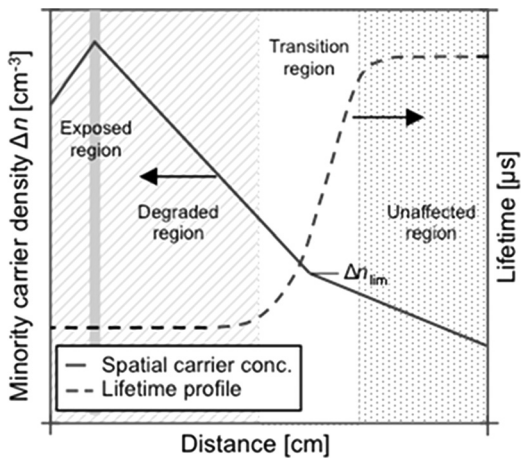

FIG. 3. Principle sketch showing the spatial carrier concentration in a sample exposed to a thin laser line. For simplicity only half of the lifetime groove is illustrated. The continuous line shows the spatial carrier concentration and the dashed line shows the spatial lifetime profile. The figure shows four regions; the shaded region corresponds to the degraded region, the grey to the exposed, the white to the transition region and the dotted to the unaffected region. The duration of the exposure determines the depth of the lifetime groove.

The basis for the simulations are; (i) a calibrated PL image of the lifetime groove measured by conventional PL imaging (5 s) where another (integrated) laser, with a wavelength of 808 nm, is used to expose the entire wafer and the resulting band-to-band PL signal is measured by a one-megapixel silicon CCD camera, and (ii) two QssPC measurements of the sample performed at $t = 0$ and $t = 10$ min illumination.

III. DATA ANALYSIS AND SIMULATIONS

The goal of the simulations and analysis presented here is to determine the value of Δn_{lim}. As explained in Sec. III, the minority carrier density in the transition region during the spot illumination is too low to be measured directly with the PL imaging setup. Therefore, we rely on simulations of the minority carrier profile, which is determined by measurements of the lifetime spatial profile and injection-level dependence before and after illumination.

The simulations of the spatial carrier concentration profile are based on the 2D continuity equation, describing a plane (x,z) normal to the focused laser line,

$$G(x,z) + D_n \nabla^2 \Delta n(x,z) - \frac{\Delta n(x,z)}{\tau(\Delta n, x)} = 0, \qquad (1)$$

where D_{n} is the electron diffusion length. The generation rate $G(\mathrm{x,z})$ for the focused laser line is given by

$$G(x,z) = (1 - R_\lambda)\phi \exp\left(-\left(\frac{x}{\sigma}\right)^2\right)\alpha_\lambda \exp(-\alpha_\lambda z). \qquad (2)$$

Here α_λ is the attenuation coefficient for silicon, and R_λ is the reflectance at the laser wavelength ($\lambda = 780$ nm). The peak photon flux ϕ and Gaussian beam half width σ were measured by a beam profilometer and a calibrated photo spectrometer to be $\phi = 2.9 \times 10^{16}\,\mathrm{s}^{-1}\,\mathrm{cm}^{-2}$ and $\sigma = 50 \pm 5\,\mu$m for the spot used during the 10 min of light soaking. This illumination generates the defects and hence creates a spatial lifetime profile that reflects the carrier concentration profile during illumination. The carrier density in steady state is approximately homogeneous in the z-direction (depth of the sample), so the resulting carrier density values from the simulations are integrated throughout the thickness of the sample and reported only as function of x.

After the light soaking, the *spatial dependence of the lifetime* is determined by acquiring a standard PL lifetime image. The procedure to extract the true spatial lifetime profile from the diffusion-affected PL image is described in Ref. 7. This yields a sigmoidal curve that rises from a low lifetime plateau τ_{low} near the spot location to a high lifetime plateau τ_{high} far away from the spot, as sketched in Fig. 3.

The *injection level dependence* is determined by QSSPC measurements on the samples in their deactivated state, and after being light soaked for 10 min with a halogen lamp illuminating the whole sample. The light source is intense enough to reach the regime of constant defect generation, and the sample temperature change due to the illumination is negligible. The QSSPC data obtained before light soaking (deactivated sample) are then representative for the injection level

dependence of the lifetime in the unaffected region ($\tau_{high}(\Delta n)$), far away from the laser spot ($x \gg \sigma$). The QSSPC data obtained after light soaking are representative for the low-lifetime ($\tau_{low}(\Delta n)$) plateau near the spot. An example of such measurements is shown in Fig. 4. For the transition region, the lifetime is assumed to follow the sigmoidal shape determined from the standard PL lifetime image, but with $\tau_{low}(\Delta n)$ and $\tau_{high}(\Delta n)$ lifetimes adjusted by the injection dependence. The QSSPC data are fitted to a lifetime model to obtain values below the detection limit in the low-injection regime. The effective lifetime of the samples is typically not perfectly uniform, due to surface scratches and damage to the passivation layers caused by handling. Thus, the area-averaged QSSPC lifetime is lower than the lifetime in the spot-illuminated areas. The latter are measured in as homogeneous areas as possible to avoid discrepancies with the simulations. A factor is introduced to scale the averaged QSSPC lifetime to the PL-determined lifetime in the uniform region. The assumption is then that the injection level dependence measured by QSSPC is representative also for the small uniform area probed by the focused line laser.

With $\tau(\Delta n,x)$ and $G(x,z)$ determined from measurements, Eq. (1) is solved numerically using the partial differential equation solver FlexPDE.[14] The carrier concentration limit, Δn_{lim}, is extracted from the simulated carrier profile by fitting two exponentially decaying curves to the regions corresponding to the two lifetime plateaus. In this low-injection regime (of constant lifetime with injection level) the decay constant of each fitted curve corresponds to the diffusion length in the corresponding region. The limit, Δn_{lim}, is extracted from the carrier profile curve where the normal of the simulated curve crosses the intersection of the two fitted curves, see Fig. 5.

The simulations are verified by comparison to a measurement carried out with a laser line spot of higher intensity than the one used during the light soaking. A laser line spot with peak flux of $\phi_{high} = 1 \times 10^{18}\,s^{-1}\,cm^{-2}$ and $\sigma = 50 \pm 5\,\mu m$ Gaussian half width was used during acquisition of the spatial carrier concentration profiles. Fig. 6 shows an example where the simulation fits well to the measured carrier concentration profile. The noise floor around $\Delta n = 5 \times 10^{12}\,cm^{-3}$ is also visible.

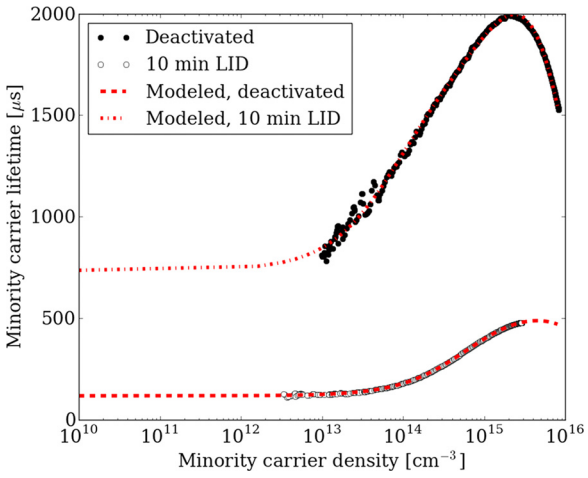

FIG. 4. Example of QSSPC measurements before and after light soaking for 10 min with a normal halogen lamp illuminating the whole sample.

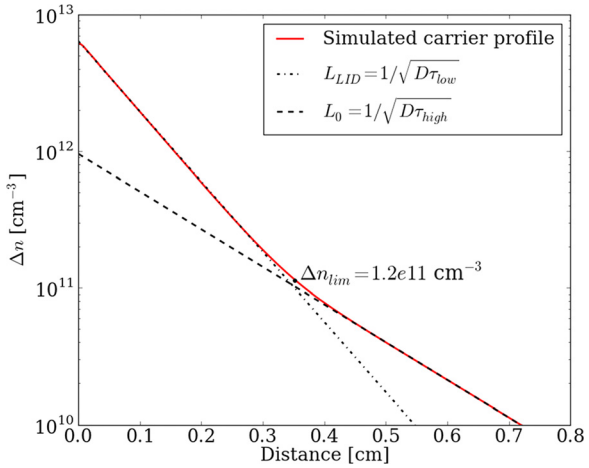

FIG. 5. Simulated carrier profile for the low-flux beam exposure at which the 10 min degradation was performed. The intersection of the two exponential curve fits (dashed lines) gives the *carrier concentration limit*, Δn_{lim}.

The simulation and analysis procedure are summarized below

1. The *spatial profile of the lifetime* is obtained from a calibrated PL image taken after 10 min spot illumination at low photon flux, ϕ_{low}.
2. The *injection level dependence* of the lifetime is determined by QSSPC measurements of the samples in their deactivated state and after 10 min light soaking.
3. The *continuity equation is solved numerically*, with the spatial and injection level dependent lifetime data from points 1 and 2.
4. The *carrier concentration limit, Δn_{lim}, is extracted* from the simulated carrier profile.

IV. RESULTS AND DISCUSSION

A. Direct monitoring of locally injected carriers

In this work, a region of light induced degraded lifetime is generated by locally exposing a sample to a low-flux laser beam. The regions of interest are the degraded, the

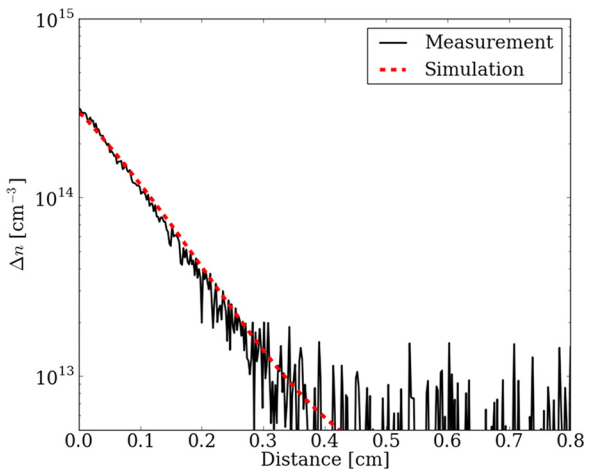

FIG. 6. Verification of the employed model. The black curve corresponds to a measurement of the spatial carrier profile carried out with the high-flux laser beam. The dashed curve corresponds to Eq. (2) with $\tau(\Delta n, x)$ and $G(x, z)$ determined from measurements.

unaffected and the transition region, where the lifetime changes (see Fig. 3). By a new method, described in the previous sections, we monitor the minority carrier density directly by photoluminescence imaging. By exciting a large enough concentration of carriers to detect the subsequent PL signal, we can observe what happens to the carrier concentration in the regions of interest. As already discussed, the actual values for Δn_{lim} are too low to be measured directly, but carrier profiles generated by a high-flux laser provide valuable information as well. The diffusion length of the material is given directly by the slope of the measured spatial carrier profile independently of the excited carrier concentration. By analyzing the slope of the spatial carrier concentrations generated by the high-flux laser, changes in the diffusion lengths can be identified. In Fig. 7, two spatial carrier profiles, generated by a high-flux laser beam, at two different positions x, are plotted. The grey carrier concentration profile is resulting from a high-flux laser line positioned in $x = 0$, but the carrier concentration is not high enough to reach the transition region before the PL detection limit is reached. The slope of the profile is, however, completely uniform demonstrating that the diffusion length in this region is uniform. This proves that above a certain Δn_{lim}, the B-O defect generation rate is fully independent of the carrier concentration and that the assumption of a lifetime plateau, inside the degraded region, used in Sec. III is correct.

The black carrier concentration profile in Fig. 7 is generated by moving the high-flux laser beam closer to the transition region. This time the carrier concentration is high enough to reach the transition region before the PL detection limit is reached. The detection of the direct PL signal in the transition region at high injection must be performed very quickly in order to not degrade the transition region, which is highly sensitive to degradation by excess carriers. Even though we use an exposure time of 15 s, we are still able to observe a change in the slope of the profile. The x-position of the change in the slope is determined by fitting two exponentially decaying curves to the right side of the decaying carrier profile. The intersection between these two curves corresponds well to the transition region of the measured lifetime profile, where the lifetime changes from being degraded to unaffected by the carrier concentration, given by the dashed curve. This finding shows that there exists a carrier threshold value at which the generation rate of B-O defects is no longer limited by carrier access.

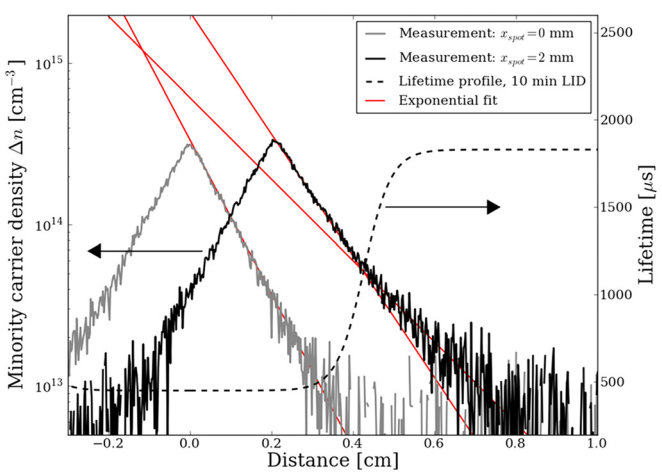

FIG. 7. Figure showing measured minority carrier density and lifetime after 10 min of low-flux laser beam exposure in $x = 0$ for a given sample. The grey curve corresponds to the carrier density profile when the high-flux laser beam is positioned in $x = 0$ and the black curve when the beam is positioned at $x = 0.2$ cm. Two individual exponential fits are shown on the $x = 0.2$ mm curve. The intersection of these fits gives the x position of where the diffusion length of the excess carriers changes. The dashed line is the measured lifetime profile.

B. Comparison of Δn_{lim} for different $N_{t\ rapid}^{*}$

The carrier concentration limit, Δn_{lim}, is extracted from the simulated carrier profiles, according to the method described in Sec. III, for a set of six samples with different doping and normalized defect concentration, N_t^*. In this study the Δn_{lim} values have been determined after exposing the samples for 10 min with a localized laser beam. This time is chosen for different reasons; (i) After 10 min, a lifetime groove with a well-defined shape is formed, suitable to test whether the slope of the spatial carrier profile will change in the transition from the degraded to the unaffected region. (ii) At 10 min small concentrations, $\Delta n < \Delta n_{\text{lim}}$, have not yet had time to cause significant degradation in the transition region, which would complicate the understanding of the spatial lifetime profile.[7] (iii) The lifetime profile after 10 min exposure is a result of the injection history during the whole 10 min exposure sequence. This means that at $t = 0$, when the lifetime of the sample is not yet degraded, the carrier concentration will be larger for all x-positions. A large difference in the diffusion length of the carriers is, however, only significant during the first few seconds of the exposure and according to previous work,[7] it was found that the extension of the degraded lifetime plateau does not change considerably over time. It is therefore realistic to employ the determined Δn_{lim} at 10 min as the actual threshold value for the Δn dependence of the B-O defect generation rate. (iv) To ease the interpretation of the results, it is convenient to look at one degradation mechanism at a time; At 10 min, the rapid degradation is complete, while the slow degradation is not yet evident. This is demonstrated in Fig. 8 where the normalized defect concentration N_t^* is plotted as a function of time for the samples of interest in this study. Accordingly, we can relate our measurement results to the rapid decay alone.

Individual Δn_{lim} values determined for each material together with their respective error bars are plotted in Fig. 9 as a function of the normalized defect concentration for the rapid decay, $N_{t\ rapid}^*$. The black error bars give the uncertainty of Δn_{lim} when the uncertainties of the calibration factor and the QSSPC measurements are taken into account. The red error bars indicate when the measurement with high-flux laser deviates from the simulation results. As can be seen from Fig. 9, the right-most point deviates quite substantially. This sample is the sample corresponding to $[\text{B}] = 8.4 \times 10^{11}$ cm^{-3} in Fig. 8. In Fig. 8, we see that at 10 min the slow degradation decay has already started for this specific sample. This might explain the deviation in simulation result to high-flux laser measurement. The deviations in the low-flux simulations are, however, expected to deviate much less from the experimental values,

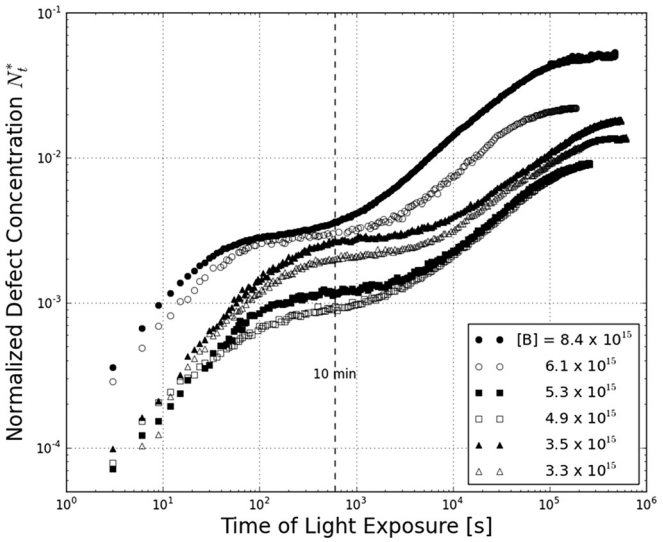

FIG. 8. Normalized defect concentration plotted as function of time for the six uncompensated boron-doped Cz-Si samples investigated in this study. The doping concentrations are given in the legend.

as the carrier lifetime is independent of the carrier injection level in this injection region.

C. Physical interpretation of Δn_{lim}

There is no indication of any obvious correlation between Δn_{lim} and $N_{t\ rapid}^{*}$ in the plot in Fig. 8. This signifies that the amount of carriers required to enable the degradation rate at full speed is independent of how many latent rapid B-O defect centres that occur in the sample. The finding is in agreement with a model where the activation is attributed to the change of the charge-state occurring when the electron quasi-Fermi level shifts across the energy level of the latent centre in its passive state. The determined Δn_{lim} concentration enables us to determine this energy level directly, since the Δn_{lim} concentration corresponds to the quasi-Fermi level at which a further

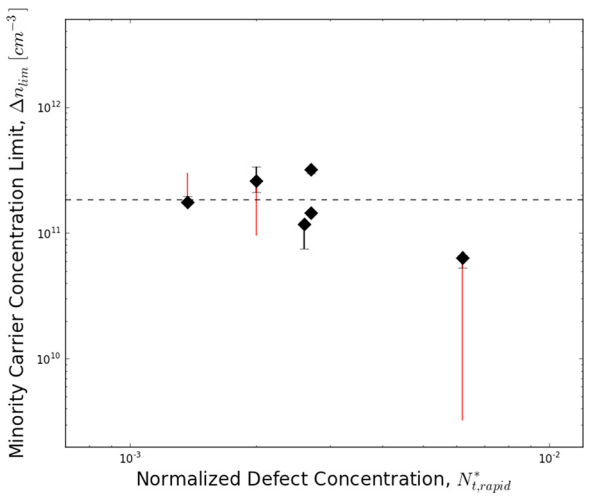

FIG. 9. Figure showing the minority carrier concentration limit, Δn_{lim}, as a function of N_t^* rapid. No correlation between Δn_{lim} and N_t^* can be observed. The black error bars give the uncertainty of Δn_{lim} when the uncertainties of the calibration factor and the QSSPC measurements are taken into account. The red error bars indicate when the measurement with high-flux laser deviates from the simulation results.

rise in the band gap will not cause any further increase in the defect generation rate. This is, however, only true if the equilibrium constant, k, of the charge state reaction $LC + e^- \leftrightarrow LC^-$ is sufficiently high (LC = Latent Centre). If k is $\ll 1$, it is possible that the defect energy level is positioned lower in the band gap and that an increase in the quasi-Fermi energy above this level simply causes an increase in k. This scenario cannot, however, be correct according to a measurement by Bothe,[15] where sub band gap illumination was used. In the first case, photons with energy above 0.50 eV were blocked. In this case, no defects were created. Subsequently, photons with energy above 0.73 eV were blocked and the experiment was repeated. In this case, defect generation was observed. Thus, the energy level must lie in between these limits. The determined Δn_{lim} concentration therefore enables us to determine the quasi-Fermi level responsible for the charge-state change of the latent defect centre directly.

The arithmetic average Δn_{lim} concentration from the measurement series shown in Fig. 9 is given by the dashed line and yields $\Delta n_{\text{lim}} = 1.84 \pm 0.9 \times 10^{11}\,\text{cm}^{-3}$. The quasi-Fermi energy from this concentration gives $E_{\text{lat}} = E_{\text{V}} + (635 \pm 18)$ meV determined by[16]

$$E_F{}^n - E_i = kT \times \ln\frac{n}{n_i}, \tag{3}$$

where E_{F}^{n} is the quasi-Fermi energy level for the electrons in this case equivalent to E_{lat}, E_{i} is the intrinsic Fermi energy (eV), k is the Boltzmann's constant, T is the temperature, n is the electron concentration in this case equivalent to Δn_{lim}, and n_{i} is the intrinsic concentration of electrons. Previously, Bothe *et al.*[2] have determined this level by a fundamentally different route, including temperature dependence on forward bias induced open circuit voltage degradation and PC1D simulations. They calculated the level to be $E_{\text{lat}} = E_{\text{V}} + (635 \pm 20)$ meV which is in good agreement with our result. The activation of the fast recombination centre is thus after all likelihood attributed to the change of the charge-state occurring when the electron quasi-Fermi level shifts across an energy level corresponding to the reported value. A simple recharge cannot, however, explain the complete transition from a latent to recombinative defect centre. The total supply of electrons over time under illumination is much larger than the concentration of B-O defects which is assumed to be in the order of $1 \times 10^{11}\,\text{cm}^{-3}$.[5] Accordingly, if a recharging effect was the final step in the generation of recombinative centres, the hypothetical reaction $LC + e^- \leftrightarrow RC$ (RC = Recombinative Centre) should be complete almost immediately. From Fig. 8, we see that this is not the case. The normalized rapid defect concentration does not saturate until approximately 200–300 s. Thus, the charging of the latent defects cannot be the last step before a final recombinative complex is in place. Another rate limiting event, when $\Delta n > \Delta n_{\text{lim}}$, must be occurring subsequently after the recharging. This is in correspondence to the model proposed by Voronkov *et al.*[8]

V. CONCLUSION

We have developed a new method based on photoluminescence imaging to directly monitor the excess carrier

density during light induced degradation. The laser used for light soaking is continuously exposing the sample to light, generating a spatially varying profile of activated B-O defects. By this method, we show experimentally that above a certain minority carrier concentration limit, Δn_{lim}, the B-O defect generation rate is fully independent of the minority carrier concentration. By simulation, we are able to determine the carrier concentration where the generation rate of the B-O defect saturates, $\Delta n_{\mathrm{lim}} = 1.84 \pm 0.9 \times 10^{11}\,\mathrm{cm}^{-3}$. Our results are consistent with a model where the role of the excess carriers during the rapid decay is to change the charge state of the defects by shifting the electron quasi-Fermi level across the energy level of the centre in its passive state. The energy level of the passive state of the latent defect centre is determined and yields $E_{\mathrm{lat}} = E_{\mathrm{V}} + (635 \pm 18)$ meV.

ACKNOWLEDGMENTS

This project has been funded by "The Norwegian Research Centre for Solar Cell Technology" and REC Wafer, REC Solar, Elkem Solar and the Norwegian Research Council through the KMB project "Defect engineering for crystalline silicon solar cells." H. Angelskår acknowledges funding from "The Norwegian Research Centre for Solar Cell Technology" (Project No. 193829).

Birger Retterstøl Olaisen is acknowledged for making the program performing the time-resolved LID with QSSPC measurements. Helge Malmbekk for valuable discussions on trap levels in the band-gap, Jo Gjessing for help with the photon flux measurements and Halvard Haug for help with surface passivation.

[1]H. Fischer and W. Pschunder, in *Proceedings of the 10th IEEE Photovoltaic Specialists Conference*, Palo Alto, CA (IEEE, New York, 1973), p. 404.
[2]K. Bothe and J. Schmidt, J. Appl. Phys. **99**, 013701 (2006).
[3]J. Schmidt and K. Bothe, Phys. Rev. B **69**, 024107 (2004).
[4]L. I. Murin, Appl. Phys. Lett. **98**, 182101 (2011).
[5]V. V. Voronkov and R. Falster, J. Appl. Phys. **107**, 053509 (2010).
[6]V. V. Voronkov, R. Falster, K. Bothe, B. Lim, and J. Schmidt, J. Appl. Phys. **110**, 063515 (2011).
[7]T. U. Naerland, H. Angelskar, M. Kirkengen, R. Sondena, and E. S. Marstein, J. Appl. Phys. **112**, 033703 (2012).
[8]K. Bothe, R. Hezel, and J. Schmidt, Appl. Phys. Lett. **83**, 1125 (2003).
[9]V. V. Voronkov, R. Falster, J. Schmidt, K. Bothe, and A. V. Batuninac, ECS Trans. **33**, 103 (2010).
[10]H. Hashigami, Y. Itakura, and T. Saitoh, J. Appl. Phys. **93**, 4240 (2003).
[11]M. Kessler, T. Ohrdes, P. P. Altermatt, and R. Brendel, J. Appl. Phys. **111**, 054508 (2012).
[12]W. Shockley and W. T. Read, Phys. Rev. **87**, 835 (1952).
[13]K. Bothe, J. Schmidt, and R. Hezel, in *Proceedings of the 3rd World Conference on Photovoltaic Energy Conversion*, Osaka, Japan, 2003, p. 1077.
[14]Flexpde 6, PDE Solutions Inc.
[15]K. Bothe, Ph.D. The University of Hannover, 2006.
[16]D. A. Neamen, *Semiconductor Physics and Devices: Basic Principles* (McGraw-Hill, New York, 2012).